Kinetically Enhanced Reaction Pathway to Form Highly Crystalline Layered $LiCoO_2$ at Low Temperatures Below 300 ° C

Maeda, Rannosuke
Nakanishi, Ryo
Mizuhata, Minoru
Matsui, Masaki

(Citation)
Inorganic Chemistry,62(46):18830-18838

(Issue Date)
2023-10-23

(Resource Type)
journal article

(Version)
Accepted Manuscript

Kinetically Enhanced Reaction Pathway to Form Highly Crystalline Layered $LiCoO_2$ at Low Temperatures below 300 °C

Rannosuke Maeda[1], Ryo Nakanishi[1, 2],Minoru Mizuhata[1],and Masaki Matsui[1, 2, 3]*

1. Department of Chemical Science and Engineering, Kobe University, Kobe, 657-8501, JAPAN

2. Graduate School of Chemical Science and Engineering, Hokkaido University, Sapporo, 060-0810, JAPAN

3. Department of Chemistry, Hokkaido University, Sapporo, 060-0810, JAPAN

Corresponding Author

Masaki Matsui

e-mail: matsui@sci.hokudai.ac.jp

KEYWORDS
$LiCoO_2$, molten salt, flux, crystal growth, phase stability

ABSTRACT

Layered $LiCoO_2$ is usually synthesized after prolonged sintering process at high temperatures (≥ 800 °C) for 10–20 h. This study developed a "hydroflux process" to obtain a highly crystalline and layered $LiCoO_2$ at a low temperature of 300 °C within 30 min. Molten mixed hydroxide-containing water molecules significantly accelerated the formation of $LiCoO_2$, which showed a highly reversible capacity of 120 mAh g^{-1} without post-annealing. The reaction mechanism study showed fast growth of $LiCoO_2$ crystals, suggesting that the excess molten hydroxides containing water dissolve the cobalt species of $HCoO_2^-$. Consequently, the accelerated $LiCoO_2$ formation suppresses the competing reaction of Co_3O_4 formation, leading to the spinel $LiCoO_2$ formation at low temperatures. Excess water in the starting materials further accelerated the crystal growth of $LiCoO_2$, forming large particles (> 1 μm). Moreover, the layered $LiCoO_2$ began to form at 150 °C. This study is the first experimental demonstration that proves the thermodynamic stability of layered $LiCoO_2$ at low temperatures (150–300 °C) under ambient pressure. This novel process offers significant energy savings in the production process of $LiCoO_2$ and other ceramics materials.

INTRODUCTION

Lithium cobalt oxide ($LiCoO_2$, LCO) has been the most common cathode active material for lithium-ion batteries (LIBs) since the commercialization of LIBs in 1991.[1–3] LCO typically has a layered rocksalt structure with the space group $R\bar{3}m$ (Fig. 1(a)), and it is synthesized using a conventional solid-state reaction via high-temperature calcination at ≥ 800 °C for 10–20 h.[4–7] LCO also has another polymorph, a spinel framework with the space group $Fd\bar{3}m$ (Fig. 1(b)),

which is synthesized at a lower temperature of ~ 400 °C.[8–17] Therefore, the layered LCO is traditionally called the high-temperature (HT) phase, whereas the spinel LCO is called the low-temperature (LT) phase.

Conversely, first-principles calculations predicted that spinel LCO represents a metastable phase at all temperatures.[12,18] Despite the metastability of spinel-structured $Li_2Co_2O_4$, the minimal energy difference (8–20 meV/formula)[18] between the layered and spinel structures enables the formation of spinel LCO at low temperatures. A recent in situ synchrotron X-ray diffraction (XRD) study by Bai et al. revealed that the formation of metastable spinel LCO is kinetically driven by the topotactic ion-exchange reaction of Li^+/Co^{2+} from the intermediate Co_3O_4 spinel phase.[19] They also argued that the LT/HT-LCO nomenclature is misleading when considering the thermochemical point of view. The metastability of spinel LCO suggests a possible pathway to form layered LCO at low temperatures (< 400 °C).

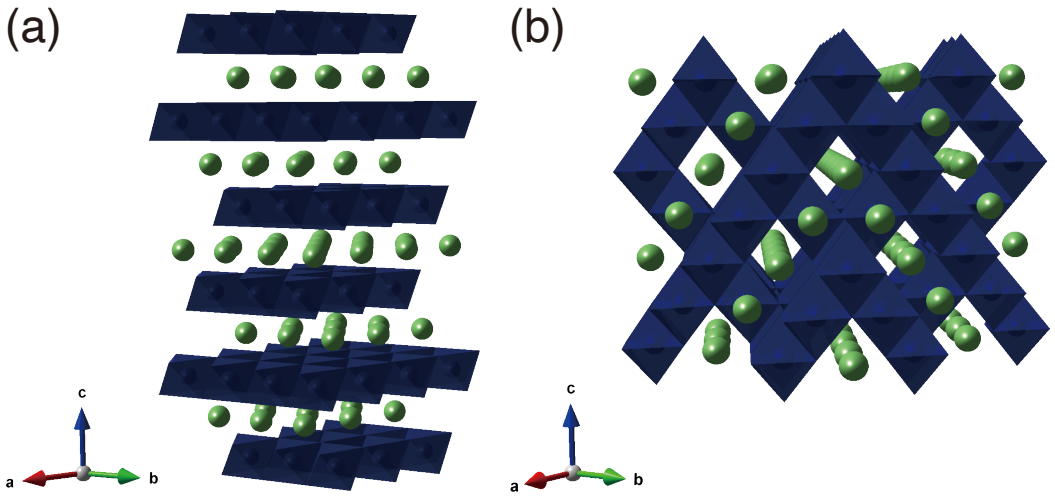

Figure 1. Crystal structure of a layered $LiCoO_2$ (a) and spinel $LiCoO_2$ (b). The crystal structures are drawn using VESTA[20]

Several research groups attempted to synthesize layered LCO using a hydrothermal reaction.[21–27] Amatucci et al. reported the successful formation of layered LCO via an ion-exchange process from CoOOH at 100 °C for 6 h.[21] Okubo et al. also synthesized layered LCO nanoparticles using CoOOH at 120–170 °C for 6 h.[22] However, despite the extended heating duration, the layered LCO synthesized in these studies exhibited poor crystallinity and required post-annealing process to improve its crystallinity.

The flux method is another synthetic approach for obtaining layered LCO at low temperatures.[28–32] Mizuno et al. obtained a highly crystalline layered LCO using the flux method at 500 °C.[29] However, a post-annealing process at ≥ 700 °C for 1 h was still required to improve the reversibility in electrochemical measurements. Therefore, the flux method offers a slight advantage over the conventional solid-state reaction.

In this study, we propose an effective synthesis approach called “hydroflux process” to obtain a highly crystalline layered LCO at low temperatures (≤ 300 °C) within a short duration of ≤ 1 h. We carefully monitored the structural evolution of the precursor materials during the synthesis to understand the reaction pathway and crystal growth process. The observed reaction pathway shows that water molecules significantly accelerate the crystal growth of layered LCO in the molten hydroxides. This study experimentally verifies that the layered LCO is a thermodynamically stable phase even at low temperatures, as predicted using theoretical calculations. The proposed hydroflux process could serve as a rapid and scalable synthetic strategy for producing layered LCO at low temperatures.

EXPERIMENTAL SECTION

Low-temperature synthesis of layered $LiCoO_2$ and product characterization

$LiCoO_2$ was synthesized via a modified solid-state reaction using cobalt hydroxide ($Co(OH)_2$, Kojundo Chemical Laboratory, 99%) and either lithium hydroxide anhydrous (LiOH) or lithium hydroxide monohydrate ($LiOH \cdot H_2O$, Wako, 99.0%) as starting materials. The LiOH was prepared by vacuum-drying $LiOH \cdot H_2O$ at 300 °C for 4 h. Sodium hydroxide (NaOH, Wako, 93.0%) and potassium hydroxide (KOH, Wako, > 85%) were added as additives to form a molten hydroxide phase during calcination.

The starting materials were thoroughly mixed in an Ar-filled glove box using an agate mortar and pestle. The Li/Co molar ratio in the mixture was fixed at 1.5:1 for all synthesis conditions, whereas the Li/Na ratio was varied. We weighed 0.70 g of $Co(OH)_2$, 0.47 g of $LiOH \cdot H_2O$, and the required amount of NaOH and KOH for each synthesis. Approximately 1.4 g of the mixed precursor was pelletized and placed on an Au foil to avoid a reaction with the alumina boat during calcination. The boat with a pellet is confined in an alumina tube with one closed end, as shown in Fig. S1. Each pellet was heated at 5 °C/min to 300 °C, held for 12 h under oxygen flow, and then cooled naturally to room temperature. The oxygen flow rate was 20 mL/min. The obtained samples were grounded and washed with anhydrous ethanol to remove excess alkaline salts three times.

The reaction pathway was investigated by freezing intermediate samples during calcination. After heating the samples to 300 °C and holding them for 0, 5, 10, 15, 20, and 30 min, the reaction was quenched by immersing the alumina tube in liquid nitrogen. The reaction temperature was varied from 100 to 300 °C. Co_3O_4 and CoO were prepared as alternative Co

sources. Co_3O_4 was synthesized by calcining $Co(OH)_2$ at 500 °C in air. To obtain the CoO rocksalt phase, $Co(OH)_2$ was calcined at 1000 °C under Ar flow.

Phase identification of the synthesized samples was performed using a laboratory X-ray diffractometer (D8 Advance, Bruker) equipped with Co Kα radiation. Structural refinement was performed using RIETAN-FP software.[33] Raman spectroscopy was performed using a triple Raman spectrometer (T-6400, Horiba-Jobin Yvon) utilizing incident radiation at 532 nm. The surface morphology was observed using field-emission scanning electron microscopy (JEM-6335F, JEOL) at an acceleration voltage of 15 kV.

Electrochemical measurements

Electrochemical measurements were conducted using a two-electrode cell (TJ-AC, Tomcell, Japan), as shown in Fig. S2. 85 wt. % of the obtained $LiCoO_2$, 10 wt. % of acetylene black (DENKA BLACK Li, Li-100, Denka), and 5 wt. % of polyvinylidene fluoride (PVdF; KF polymer #1120, KUREHA) were dispersed in N-methyl-2-pyrrolidone (NMP; WAKO Pure chemical industries) as a solvent to prepare an electrode slurry. The slurry was coated on an aluminum current collector and dried at 80 °C for 1 h. All electrodes were punched into 16-mm-diameter circular disks, pressed at 25 MPa, and dried at 120 °C for 3 h under vacuum. The resulting electrode exhibited an active material loading of 2.8–3.1 mg cm^{-2}. Additionally, half-cells with a Li metal counter electrode were fabricated. An electrolyte solution of 1 mol L^{-1} $LiPF_6$ in ethylene carbonate (EC): diethyl carbonate (DEC) at 1:1 volume ratio (Kishida Chemical) was used.

Galvanostatic charge–discharge tests were performed using a standard charger (TOSCAT-3100, Toyo System). The charge–discharge current was C/10 (1 C = 139.6 mA $g^{-1}/LiCoO_2$) based on

the theoretical capacity of $Li_{1-x}CoO_2$ ($0 \leq x \leq 0.5$), and the voltage range was between 2.5 and 4.2 V at room temperature. A series of electrochemical tests were also conducted to estimate the purity of the $LiCoO_2$ based on the theoretical capacity of 139.6 mAh g^{-1}.

Sample nomenclature

Sample names in this study refer to the composition ratio of the starting materials. Each component is represented by its abbreviation, LiOH (L), $LiOH \cdot H_2O$ (Lh), NaOH (N), KOH (K), and $Co(OH)_2$ (C), followed by its molar ratio. For example, a sample synthesized by mixing $LiOH \cdot H_2O$, NaOH, and $Co(OH)_2$ in a molar ratio of 1.5:0.5:1 is denoted as Lh1.5N0.5CO. The letter O stands for the oxide, and the molar ratio is normalized to a Co content of 1. A detailed list of the composition ratios is provided in Table S1. In addition, all the samples synthesized via the LiOH-NaOH binary system are plotted on the phase diagram, as shown in Fig S4. [34,35] Detailed experimental conditions are available in Supplementary Note 1.

RESULTS AND DISCUSSION

Synthesis and characterization of $LiCoO_2$

Our proposed synthetic approach was based on two ideas. One involves the in situ ion-exchange process via the formation of layered O3-type $NaCoO_2$ at around 250 °C.[36–38] The other involves enhancing the reaction kinetics using molten hydroxide. NaOH is the most suitable additive for realizing both concepts. The LiOH-NaOH binary hydroxide system shows a eutectic point at 220 °C with a Li/Na molar ratio of 3/7, as shown in the binary phase diagram (Fig. S3).[34,35] Therefore, we first synthesized layered LCO at this Li/Na ratio. Figure 2 (a) shows the XRD

pattern of $LiCoO_2$ synthesized from LiOH, NaOH, and $Co(OH)_2$ at the molar ratio of 1.5/3.5/1. The obtained sample is referred to as L1.5N3.5CO, according to the nomenclature explained earlier. The broad reflection peaks were attributed to layered LCO. Even though the 006 and 102 peaks at 45–46° overlap, the 003 peak at 21.9° suggests that the primary component of the sample was layered LCO. The relatively weak peak intensity of the 104 reflection at 45° indicated the formation of spinel LCO and Co_3O_4 as byproducts. L1.5N3.5CO contains numerous stacking faults in its layered structure, because even the $Co(OH)_2$ used for synthesis exhibits superior crystallinity, as shown in Fig. S4. Raman spectroscopy analysis of the layered LCO was also performed. In Fig. 2 (b), the Raman spectrum of L1.5N3.5CO shows two bands at 487 and 597 cm^{-1}, which are assigned to the A_{1g} and E_g modes of layered LCO, respectively.[39] The weak Raman bands observed at 696, 652, and 525 cm^{-1} were assigned to Co_3O_4. [40] Raman bands at 445, 478, 583, and 603 cm^{-1} corresponding to the spinel type LCO, were not detected. The XRD and Raman results indicate that layered LCO was the thermodynamically stable phase at 300 °C. Meanwhile, Co_3O_4 formation remains a kinetically competitive reaction. Consequently, further enhancement in the reaction rate is necessary to obtain the layered LCO single phase.

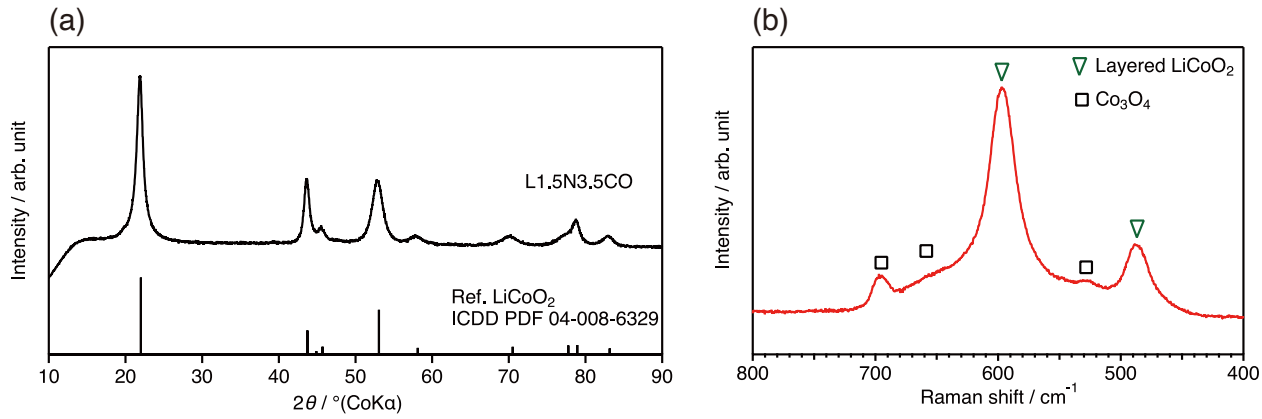

Figure 2. (a) XRD pattern and (b) Raman spectrum of $LiCoO_2$ obtained by calcining anhydrous LiOH-NaOH binary mixed hydroxide at 300 °C for 12 h

We observed that water molecules in the starting materials significantly improved the crystallinity of LCO. Figure 3 (a) shows the XRD pattern of Lh1.5N3.5CO synthesized using $LiOH{\cdot}H_2O$. The apparent splitting of the 006 and 102 reflection peaks at 45–46° and the 018 and 110 reflection peaks at 77.5–80° suggested the formation of highly crystalline and layered $LiCoO_2$. The reflection peaks at 42.7° and 49.8° were attributed to the CoO rocksalt phase formed via dehydration of $Co(OH)_2$. The CoO formation shows that excess Li in the raw materials remained unreacted as a molten hydroxide phase during calcination. The Raman spectrum of Lh1.5N3.5CO (Fig. 3(b)) shows two peaks corresponding to the A_{1g} and E_g modes of layered LCO. This observation indicates that the reaction kinetics required to form layered LCO was enhanced by water molecules in $LiOH{\cdot}H_2O$. This enhanced kinetics suppresses the competing reaction of Co_3O_4 formation effectively.

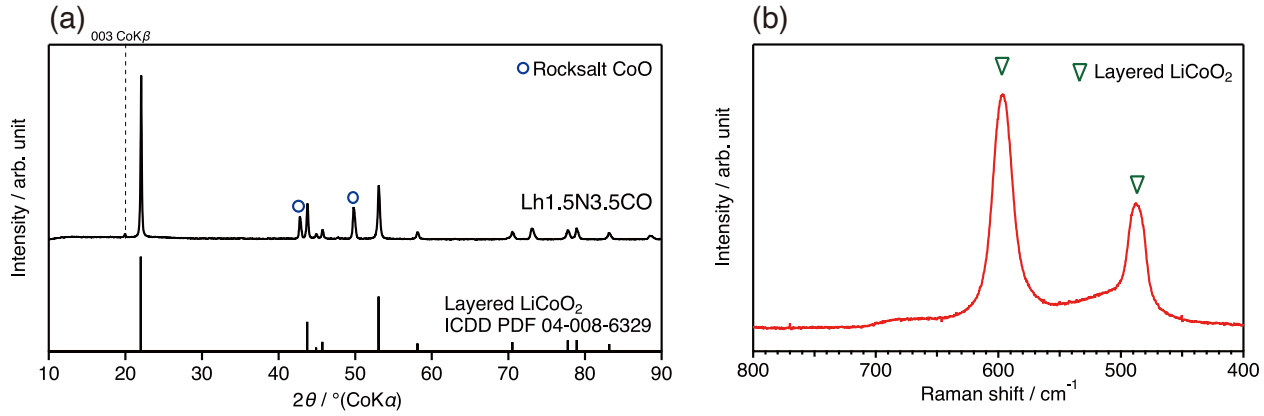

Figure 3. (a) XRD pattern and (b) Raman spectrum of $LiCoO_2$ obtained by calcining LiOH-NaOH binary mixed hydroxide containing crystal water at 300 °C for 12 h

Figure 4 shows the SEM images of $Co(OH)_2$, L1.5N3.5CO, and Lh1.5N3.5CO. The surface morphology of L1.5N3.5CO is slightly rougher than that of $Co(OH)_2$, as shown in Fig. 4(a) and (b), indicating partial phase separation of $Co(OH)_2$ during the calcination process. In contrast, Lh1.5N3.5CO comprises hexagonal plate-like particles, reflecting a hexagonal lattice structure. Some large particles (diameter = 300–500 nm) showed trace crystal growth during synthesis. The calcination temperature of 300 °C was insufficient to promote the sintering of typical transition metal oxides. Therefore, we assume that the crystal growth of layered LCO occurs via a dissolution-redeposition process in the molten hydroxides containing water.

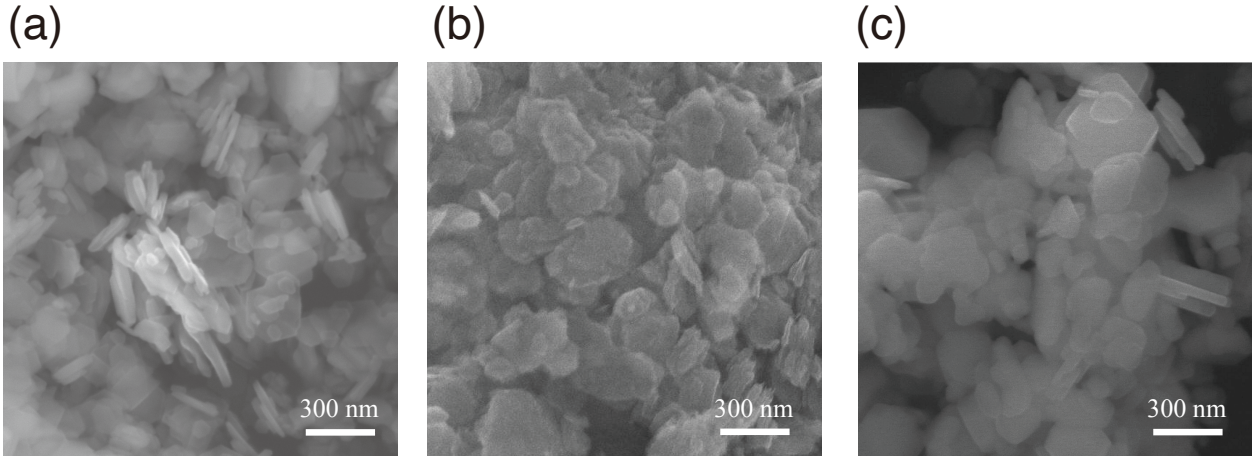

Figure 4. SEM images of (a) $Co(OH)_2$ as starting material and $LiCoO_2$ samples synthesized from (b) anhydrous molten hydroxide (L1.5N3.5CO), and (c) hydrated molten hydroxide (Lh1.5N3.5CO)

We optimized the starting materials' composition to reduce the formation of rocksalt CoO. We lowered the NaOH content to synthesize the LCO samples designated as Lh1.5N1.5CO and Lh1.5N0.5CO, as shown in Fig. S5. The rocksalt CoO content in Lh1.5N1.5CO and Lh1.5N0.5CO was successfully decreased as expected. The optimization process showed us that increasing the lithium activity in the molten hydroxide was crucial to obtaining a pure LCO phase. Furthermore, the poor crystallinity of the NaOH-free sample (Lh1.5CO) also suggested that crystal growth occurs via the liquid phase. The detailed optimization process is described in Supplementary Note 2.

We also performed Rietveld refinement to evaluate the quality of the obtained material. The structural refinement result of Lh1.5N0.5CO is shown in Fig. 5(a). This sample exhibited a layered LCO phase with the space group $R\bar{3}m$ and lattice constants of a = 2.8176 Å and c =

14.0587 Å. Because these lattice parameters align with those obtained in a reported single-crystal XRD analysis[41], the concentration of lattice defects, such as oxygen vacancies and cation mixing, was negligible. The structural refinement result shows that 2.49 mol% of rocksalt CoO remained unreacted. Detailed results of the structural refinement are summarized in Table 1. The improved crystallinity of the Lh1.5N0.5CO sample was also confirmed using the SEM image in Fig. 5(b). Large hexagonal particles (> 1.0 μm) were observed in the SEM image, suggesting a crystal growth during calcination. Further improvements in reaction uniformity will yield more crystalline particles.

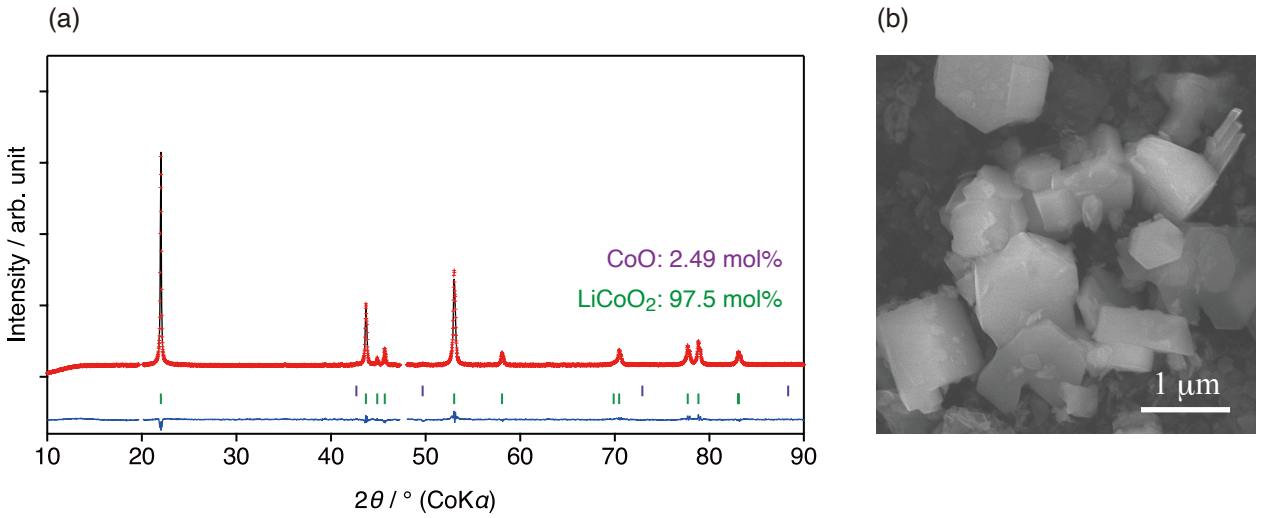

Figure 5. (a) Rietveld refinement result of Lh1.5N0.5CO. Red crosses: experimental data, black line: fitting result, blue line: residue of the fitting, green ticks: peak positions of $R\bar{3}m$ layered $LiCoO_2$, and magenta tick: peak positions of $Fm\bar{3}m$ CoO rocksalt phase. (b) SEM image of Lh1.5N0.5CO, showing large crystalline particles of $LiCoO_2$

Table 1. Rietveld refinement result of Lh1.5N0.5CO

(A) Crystallographic data of $LiCoO_2$ and CoO						
$LiCoO_2$, Trigonal, $R\bar{3}m$ (No. 166)						
a / Å	b / Å	c / Å	α / °	β / °	γ / °	V / Å^3
2.81761(5)	2.81761(5)	14.05870(17)	90	90	60	96.657(3)
atom	Wyckoff	X	y	z	occ	U
Li	3a	0	0	0	1	0.02533[a]
Co	3b	0	0	0.50000(14)	1	0.00633[b]
O	6c	0	0	0.24210(20)	1	0.00633[b]
CoO, Cubic, $Fm\bar{3}m$ (No. 225)						
a / Å	b / Å	c / Å	α / °	β / °	γ / °	V / Å^3
4.2571(7)	4.2571(7)	4.2571(7)	90	90	90	77.15(2)
atom	Wyckoff	x	y	z	occ	U
Co	4a	0	0	0	1	0.00633
O	4b	0.5	0.5	0.5	1	0.00633
(B) Reliability Indices						
R_{wp}	R_p	GoF	R_b $LiCoO_2$	R_b CoO		
3.969	3.045	2.953	5.158	11.228		

[a]The atomic displacement of Li was fixed to be 2.0.

[b]The atomic displacements of Co and O were fixed to be 0.5.

Electrochemical properties

We performed charge–discharge tests for $LiCoO_2$ synthesized at 300 °C without post-annealing. Fig. 6 shows the charge–discharge profiles of Li/$LiCoO_2$ half-cells using Lh1.5N0.5CO and L1.5N3.5CO in the voltage range of 2.5–4.2 V at 25 °C and C/10 (1 C = 139.6 mA g^{-1}/$LiCoO_2$). Highly crystalline Lh1.5N0.5CO shows a plateau corresponding to the $LiCoO_2$/Li_xCoO_2 redox

couple at 3.9 V, and the first charge and discharge capacities were 136 and 118 mAh g^{-1}, respectively. A small voltage step corresponding to the hexagonal/monoclinic phase transition of layered LCO was also observed at 4.1 V. The slightly low reversible capacity and continuous capacity decay were attributed to the unreacted CoO and hydroxide residue in the sample. We estimated the purity of the layered LCO to be approximately 83 wt. %. The detailed discussions to estimate the amount of impurity phase are described in Supplementary Note 3. Despite these challenges, the electrochemical behavior proves that the primary component of Lh1.5N0.5CO was layered LCO. These results agreed with the theoretical prediction that layered LCO was a thermodynamically stable phase even at low temperatures.

Conversely, the charge–discharge profiles of L1.5N3.5CO suggests that the active material contains a large amount of spinel Co_3O_4, as shown in Fig. 6(b). Lithium extraction occurred at around 3.6 V, and there was an apparent plateau once the cell reached the upper cutoff voltage of 4.2 V. The poor coulombic efficiency of 54% in the first cycle and significant capacity decay in the following cycles also showed that the primary product in L1.5N3.5CO was not layered LCO. A comparison of the electrochemical properties indicated the significant role of water molecules in layered LCO formation. Because the synthesis temperature of 300 °C was relatively high for a typical hydrothermal process but low for a flux process, we have coined the term “hydroflux process” to describe this innovative synthesis method.

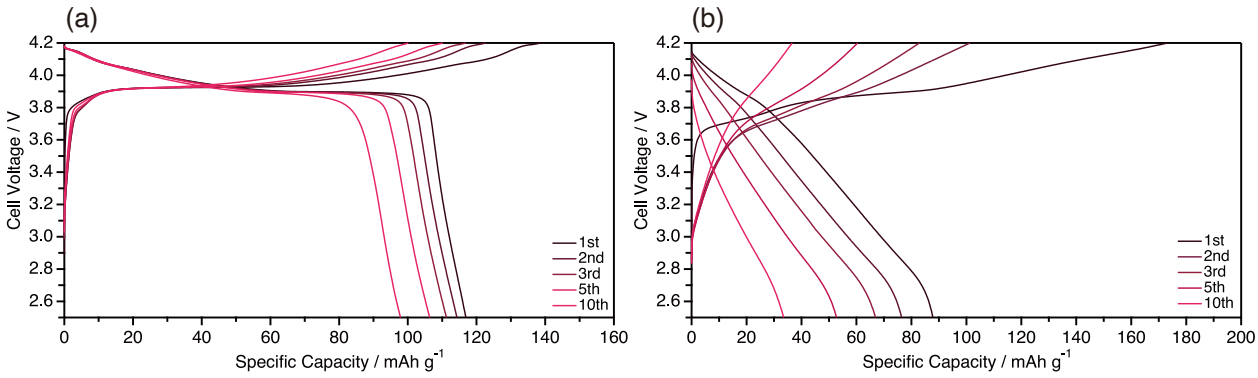

Figure 6. Charge–discharge profiles of $LiCoO_2$ synthesized at 300 °C using (a) $LiOH{\cdot}H_2O$-NaOH hydrated molten hydroxide and (b) LiOH-NaOH anhydrous molten hydroxide

Reaction pathway for low-temperature synthesis

Next, we investigated the reaction pathways to understand the role of the water molecules. We tried to detect the intermediate species by quenching the samples during calcination and analyzing them through ex situ XRD analysis. Figure 7 shows the phase evolution during the calcination of Lh1.5N0.5CO as the starting material. The XRD pattern of the starting materials did not contain peaks corresponding to $LiOH{\cdot}H_2O$ or NaOH, suggesting that NaOH dehydrated $LiOH{\cdot}H_2O$. After 10 min, the XRD pattern revealed decaying peak intensities of $Co(OH)_2$, and new peaks attributed to rocksalt-structured CoO occurred at $2\theta = 43°$ and 50°. Small amounts of layered $LiCoO_2$ and $NaCoO_2$ were also observed. After 15 min, the peaks attributed to $Co(OH)_2$ mostly disappeared, and those attributed to CoO became significantly stronger in intensity. An additional 5 min of calcination shifted the primary phase from rocksalt CoO to layered LCO,

suggesting that the oxidation of the CoO species primarily progressed during these 5 min with simultaneous formation of layered LCO. The remaining CoO disappeared completely after 30 min. Notably, the diffraction pattern after 30 min of calcination closely resembled that after 12 h, indicating that the crystal growth of layered LCO was completed within 30 min when calcinated at 300 °C.

The CoO formation suggests that dehydration of $Co(OH)_2$: equation (1) is the immediate reaction rather than Co_3O_4 spinel formation:

$$Co(OH)_2 \rightleftharpoons CoO + H_2O \qquad (1)$$

Because the calcination temperature of 300 °C is insufficient for crystal growth in the solid phase, we think that layered LCO formation occurs via the liquid phase. Based on the Pourbaix diagram shown in Fig. S9, $HCoO_2^-$ is supposed to form as a soluble species in molten hydroxide via the following equilibrium (2):

$$CoO + OH^- \rightleftharpoons HCoO_2^- \qquad (2)$$

Subsequently, the dissolved $HCoO_2^-$ ions are oxidized and react with Li^+ ions to form layered LCO. The enhanced solubility of $HCoO_2^-$ by water molecules enabled the fast crystal growth of layered LCO even at the low temperature of 300 °C. In addition, as the solubility product of water decreased at high temperatures, the equilibrium between CoO and $HCoO_2^-$ also shifted to a lower pH. Consequently, $HCoO_2^-$ became more stable over a wide pH range in the aqueous system. Therefore, the crystal growth of layered LCO is expected to stop once water completely evaporates from the molten hydroxides. Figure S8 shows the charge–discharge profiles of

$LiCoO_2$ synthesized following calcination of Lh1.5N0.5CO at 300 °C for 30 min. The similar charge–discharge profiles further verify the fast reaction kinetics of the hydroflux process.

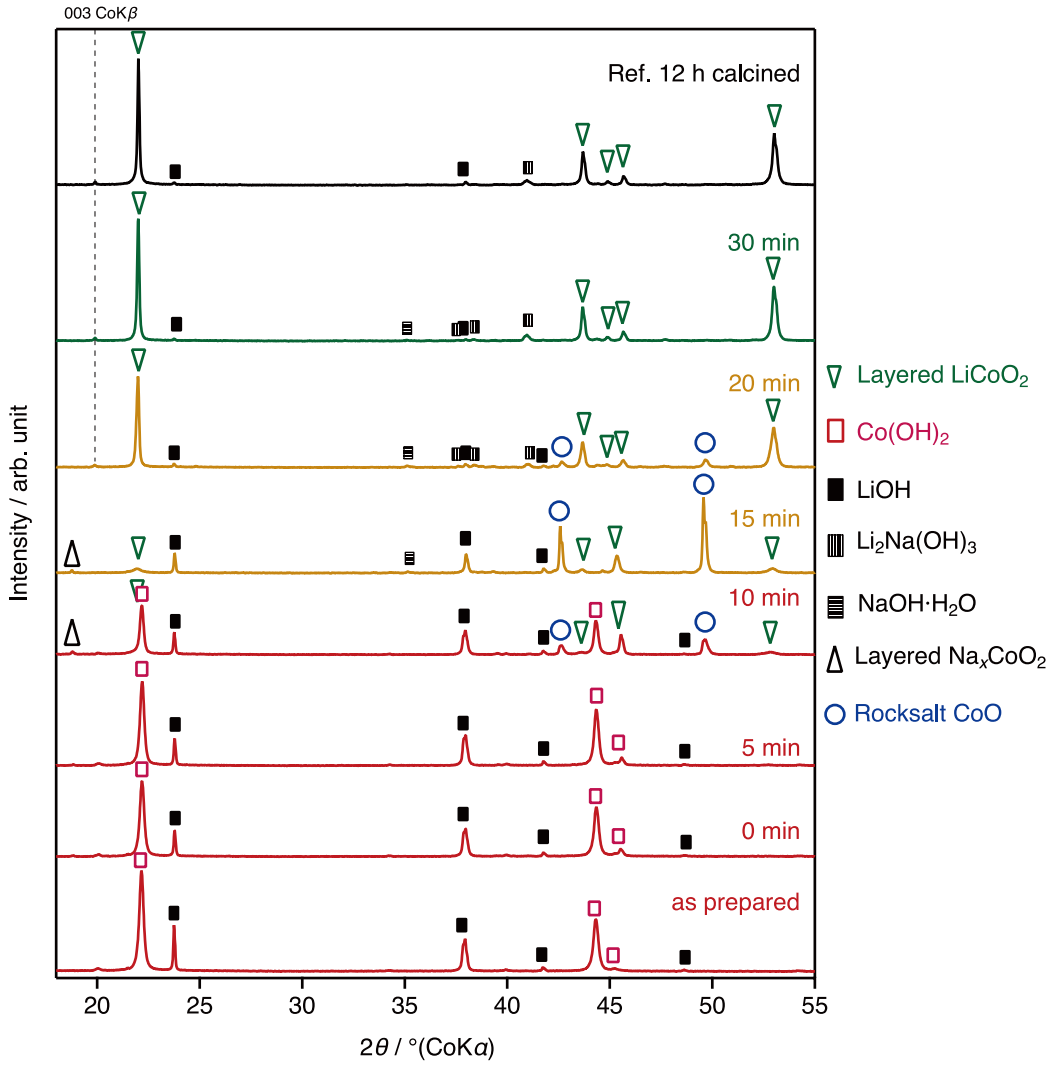

Figure 7. Phase evolution during $LiCoO_2$ synthesis at 300 °C using $LiOH·H_2O$-NaOH binary molten hydroxide. The XRD patterns were collected without EtOH rinse

We performed LT synthesis using CoO and Co_3O_4 as cobalt sources to confirm whether CoO or $HCoO_2^-$ formation was essential to obtain layered LCO. Figure 8 shows the XRD patterns of

products synthesized using CoO and Co_3O_4 as the starting materials. CoO successfully formed layered LCO, whereas Co_3O_4 remained unreacted. The unreacted CoO indicated that water molecules generated in the dehydration process of $Co(OH)_2$ also enhanced the reaction kinetics. Conversely, the poor reactivity of Co_3O_4 shows that the formation of spinel LCO was much slower than that of layered LCO from CoO.

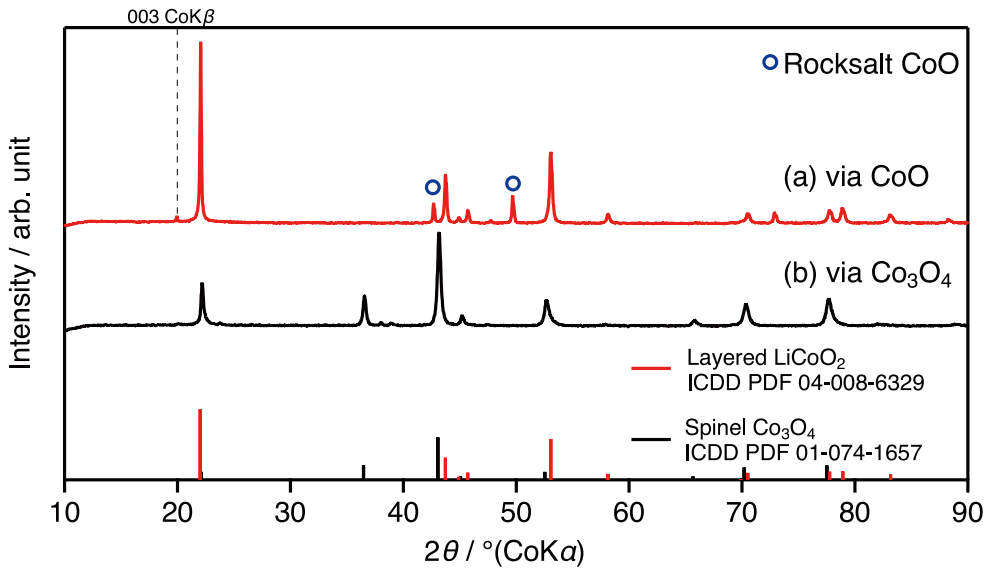

Figure 8. XRD patterns of samples synthesized via the hydroflux process at 300 °C using different cobalt sources. (a) Rocksalt CoO produced layered $LiCoO_2$, while (b) spinel Co_3O_4 failed to react

The temperature dependence of the reaction is also investigated, as shown in Fig. 9. The layered LCO was formed at 150 °C. The layered LCO formation below the eutectic point indicates the generation of a liquid phase by water molecules contained in the starting materials. The crystallinity of layered LCO significantly improved at above 250 °C, supporting the hypothesis that crystal growth of layered LCO occurred via the liquid phase containing water molecules. As

the amount of molten hydroxide increased above the eutectic point, the amount of dissolved $HCoO_2^-$ also increased.

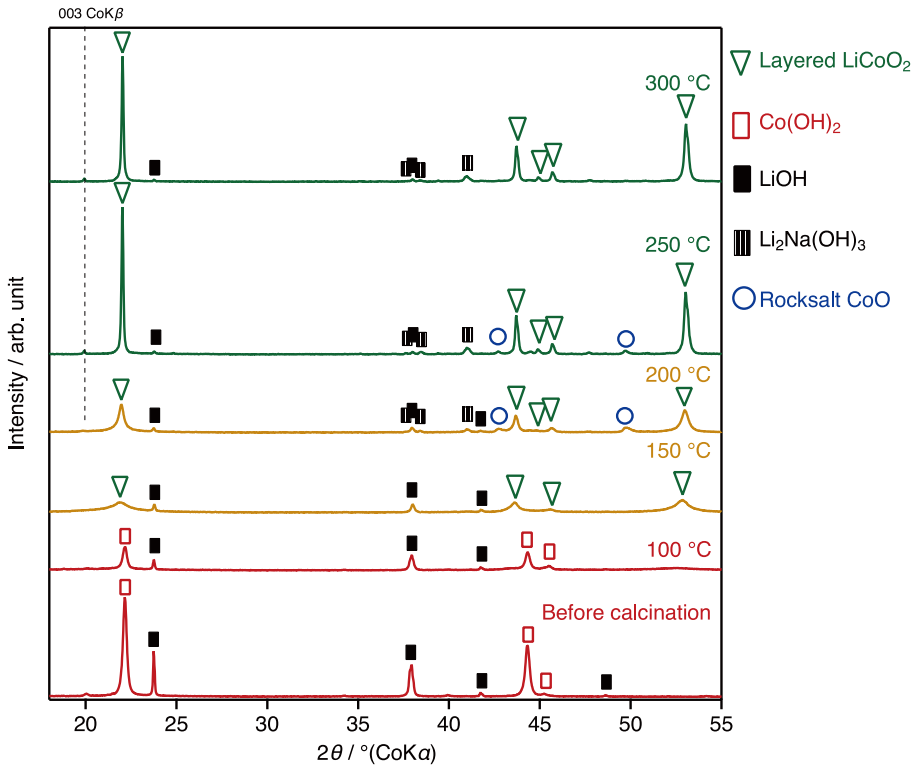

Figure 9. XRD patterns of $LiCoO_2$ synthesized via the hydroflux process for 1 h at various temperatures without EtOH rinse

To increase the amount of dissolved $HCoO_2^-$ in the molten hydroxide at low temperatures, we applied the hydroflux process using the LiOH–NaOH–KOH ternary molten hydroxide system because the eutectic point of NaOH-KOH was 170 °C (Supplementary Note 5). We successfully improved the crystallinity of the layered LCO synthesized at 200 °C using the ternary molten hydroxide system, as shown in Fig. S12. However, significant crystal growth of layered LCO was observed only above 250 °C, indicating that the solubility of the $HCoO_2^-$ improved above

200 °C. Therefore, we conclude that the activity of $HCoO_2^-$ is critical for the crystal growth process under the present synthesis conditions.

Further improvement of synthesis conditions

The above discussion indicates that dissolved $HCoO_2^-$ ions are crucial for the crystal growth of layered LCO. Therefore, we attempted to improve the solubility of $HCoO_2^-$ by adding excess water to the starting material. Figure 10 shows the structural refinement results of XRD, SEM images, and charge–discharge profiles of $LiCoO_2$ synthesized using Lh1.5N0.5CO–H_2O3.0 at 300 °C. The additional "H_2O3.0" represents the amount of excess water added to the starting materials. The fitting results are summarized in Table 2. The obtained layered LCO showed even higher crystallinity. The excess water accelerated crystal growth, forming large particles (1–2 μm). The smaller particles observed in Lh1.5N0.5CO mostly disappeared, suggesting that crystal growth of layered LCO occurred via the liquid phase.

The specific capacity of 115–120 mAh g^{-1} shows 15–20 mol% of inactive species remaining in the sample. Although the amount of the crystalline rocksalt CoO content was 0.7 mol% quantified by the Rietveld refinement, the impurity phases should be mostly non-crystalline phases, including the alkaline hydroxide residue. Despite the remaining impurity phases, the improved cycling performance indicates that the quality of the bulk LCO should be high enough. The steep voltage drop at the end of the discharging process proves that the quality of the obtained LCO was comparable to that of LCO synthesized at high temperatures. These results show that water molecules in the molten hydroxide enhanced the solubility of $HCoO_2^-$, resulting in fast crystal growth of layered LCO.

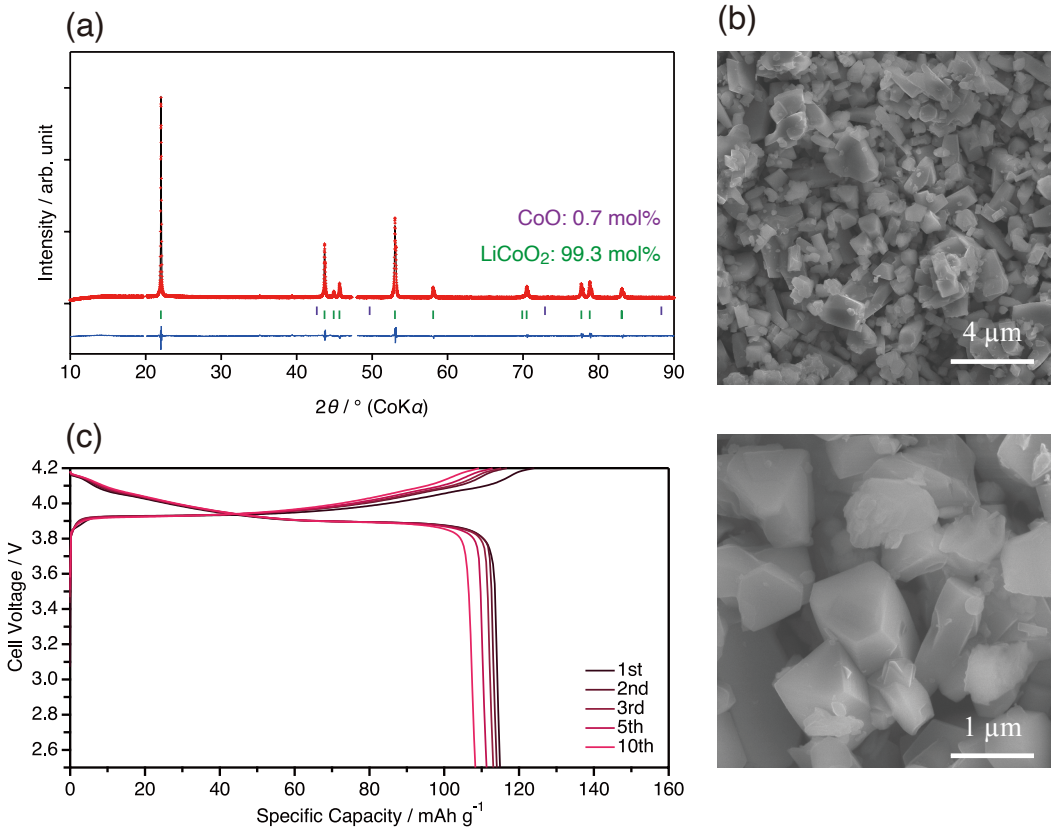

Figure 10. (a) Rietveld refinement result, (b) SEM images, and (c) charge–discharge profiles of $LiCoO_2$ synthesized via the hydroflux process at 300 °C with excess water. The excess water accelerated the crystal growth of $LiCoO_2$ according to (a) and (b). The reversibility and capacity retention were also improved according to (c)

Table 2. Rietveld refinement result of Lh1.5N0.5CO3.0H_2O

(A) Crystallographic data of $LiCoO_2$ and CoO						
$LiCoO_2$, Trigonal, $R\bar{3}m$ (No. 166)						
a / Å	b / Å	c / Å	α / °	β / °	γ / °	V / Å^3
2.81743(2)	2.81743(2)	14.05359(8)	90	90	60	96.6105(12)
Atom	Wyckoff	X	y	z	occ	U
Li	3a	0	0	0	1	0.02533[a]
Co	3b	0	0	0.50000(15)	1	0.00633[b]
O	6c	0	0	0.24210(6)	1	0.00633[b]
CoO, Cubic, $Fm\bar{3}m$ (No. 225)						
a / Å	b / Å	c / Å	α / °	β / °	γ / °	V / Å^3
4.2571(7)	4.2571(7)	4.2571(7)	90	90	90	77.15(2)
atom	Wyckoff	x	y	z	occ	U
Co	4a	0	0	0	1	0.00633
O	4b	0.5	0.5	0.5	1	0.01267
(B) Reliability Indices						
R_{wp}	R_p	GoF	R_b $LiCoO_2$	R_b CoO		
4.257	3.183	3.5252	4.141	8.270		

[a]The atomic displacement of Li was fixed to be 2.0.

[b]The atomic displacements of Co and O were fixed to be 0.5.

CONCLUSIONS

In this study, we explored a new reaction pathway to obtain highly crystalline layered $LiCoO_2$ at low temperatures of ≤ 300 °C without a post-annealing process. Mixed molten hydroxide of $LiOH{\cdot}H_2O$ and NaOH containing water significantly enhanced the solubility of the cobalt species $HCoO_2^-$, resulting in crystal growth of layered LCO via the liquid phase within a short calcination period of 30 min. We also confirmed the formation of a layered LCO at 150 °C. To our knowledge, this is the first experimental demonstration of the thermochemical stability of layered $LiCoO_2$ at low temperatures under ambient pressure.

The proposed hydroflux process has an optimal reaction temperature range of 250–300 °C, which is considerably lower than that of the conventional flux process. Within these temperature ranges, excess water in the system enhances the solubility of the metal ions and accelerates the crystal growth. Therefore, we anticipate that the quality of the product could be further improved via more precise control of vapor pressure during the heating process. The oxidation state of the metallic elements could also be controlled by the oxygen partial pressure. Because many metallic elements have soluble species in alkaline regions, the hydroflux process could also be applied to synthesizing various metal oxides, phosphates, and silicates. For example, all the 3d transition metals except scandium and titanium are applicable to this process. We believe that the low reaction temperature and fast kinetics are scalable and enable energy saving in various ceramics production processes.

ASSOCIATED CONTENT

Supporting Information

The Supporting Information is available free of charge at https://pubs.acs.org/doi.xxxxx

Details of experimental conditions: Note 1, Optimization of synthesis conditions: Note2, Semi-quantification of impurity phases: Note 3, Charge-discharge profiles of $LiCoO_2$ synthesized at 300 °C for 30 minutes, Pourbaix diagram of cobalt system, LiOH-NaOH-KOH ternary system for the hydroflux process: Note 4 and Supporting References.

AUTHOR INFORMATION

Corresponding Author

Masaki Matsui, Department of Chemistry, Hokkaido University, Sapporo, Hokkaido 060-0810, Japan; orcid.org/0000-0003-1499-7457; E-mail: matsui@sci.hokudai.ac.jp

Authors

Rannosuke Maeda – Department of Chemical Science and Engineering, Kobe University, Kobe, Hyogo 657-8501, Japan

Ryo Nakanishi – Graduate School of Chemical Science and Engineering, Hokkaido University, Sapporo, Hokkaido 060-0810, Japan

Minoru Mizuhata – Department of Chemical Science and Engineering, Kobe University, Kobe, Hyogo 657-8501, Japan

ACKNOWLEDGEMENTS

This study was supported by KAKENHI from MEXT (Grant Numbers 19H05812 and 19H05813) and JSPS KAKENHI (Grant Number 18K19131).

REFERENCES

(1) Goodenough, J. B.; Kim, Y. Challenges for Rechargeable Li Batteries. *Chemistry of Materials* **2010**, *22* (3), 587–603. https://doi.org/10.1021/CM901452Z/ASSET/IMAGES/LARGE/CM-2009-01452Z_0018.JPEG.

(2) Yoshino, A. The Birth of the Lithium-Ion Battery. *Angewandte Chemie International Edition* **2012**, *51* (24), 5798–5800. https://doi.org/https://doi.org/10.1002/anie.201105006.

(3) Lyu, Y.; Wu, X.; Wang, K.; Feng, Z.; Cheng, T.; Liu, Y.; Wang, M.; Chen, R.; Xu, L.; Zhou, J.; Lu, Y.; Guo, B. An Overview on the Advances of $LiCoO_2$ Cathodes for Lithium-Ion Batteries. *Adv Energy Mater* **2021**, *11* (2), 2000982. https://doi.org/https://doi.org/10.1002/aenm.202000982.

(4) Mizushima, K.; Jones, P. C.; Wiseman, P. J.; Goodenough, J. B. Li_xCoO_2 ($0<x<-1$): A New Cathode Material for Batteries of High Energy Density. *Mater Res Bull* **1980**, *15* (6), 783–789. https://doi.org/https://doi.org/10.1016/0025-5408(80)90012-4.

(5) Mizushima, K.; Jones, P. C.; Wiseman, P. J.; Goodenough, J. B. Li_xCoO_2 ($0<x\leqslant1$): A New Cathode Material for Batteries of High Energy Density. *Solid State Ion* **1981**, *3–4*, 171–174. https://doi.org/https://doi.org/10.1016/0167-2738(81)90077-1.

(6) Reimers, J. N.; Dahn, J. R. Electrochemical and In Situ X-Ray Diffraction Studies of Lithium Intercalation in Li_xCoO_2. *J Electrochem Soc* **1992**, *139* (8), 2091–2097. https://doi.org/10.1149/1.2221184.

(7) Ohzuku, T.; Ueda, A. Solid-State Redox Reactions of $LiCoO_2$ (R3m) for 4 Volt Secondary Lithium Cells. *J Electrochem Soc* **1994**, *141* (11), 2972–2977. https://doi.org/10.1149/1.2059267.

(8) Gummow, R.; Thackeray, M.; David, W.; Hull, S. Structure and Electrochemistry of Lithium Cobalt Oxide Synthesized at 400°C. *Mater Res Bull* **1992**, *27* (3), 327–337. https://doi.org/10.1016/0025-5408(92)90062-5.

(9) Gummow, R. J.; Liles, D.; Thackeray, M. Spinel versus Layered Structures for Lithium Cobalt Oxide Synthesized at 400°C. *Mater Res Bull* **1993**, *28* (3), 235–246. https://doi.org/10.1016/0025-5408(93)90157-9.

(10) Rossen, E.; Reimers, J. N.; Dahn, J. R. Synthesis and Electrochemistry of Spinel LT $LiCoO_2$. *Solid State Ion* **1993**, *62* (1), 53–60. https://doi.org/https://doi.org/10.1016/0167-2738(93)90251-W.

(11) Garcia, B.; Farcy, J.; Pereira-Ramos, J. P.; Perichon, J.; Baffier, N. Low-Temperature Cobalt Oxide as Rechargeable Cathodic Material for Lithium Batteries. *J Power Sources* **1995**, *54* (2), 373–377. https://doi.org/10.1016/0378-7753(94)02105-C.

(12) Wolverton, C.; Zunger, A. Cation and Vacancy Ordering in Li_xCoO_2. *Phy Rev B* **1998,** *57*, 2242.

(13) Antolini, E. $LiCoO_2$: Formation, Structure, Lithium and Oxygen Nonstoichiometry, Electrochemical Behaviour and Transport Properties. *Solid State Ion* **2004**, *170* (3–4), 159–171. https://doi.org/10.1016/J.SSI.2004.04.003.

(14) Choi, S.; Manthiram, A. Synthesis and Electrochemical Properties of $LiCo_2O_4$ Spinel Cathodes. *J Electrochem Soc* **2002**, *149* (2), A162. https://doi.org/10.1149/1.1431574.

(15) Ariyoshi, K.; Yuzawa, K.; Yamada, Y. Reaction Mechanism and Kinetic Analysis of the Solid-State Reaction to Synthesize Single-Phase $Li_2Co_2O_4$ Spinel. *The Journal of Physical Chemistry C* **2020**, *124* (15), 8170–8177. https://doi.org/10.1021/acs.jpcc.0c01115.

(16) Wolverton, C.; Zunger, A. Prediction of Li Intercalation and Battery Voltages in Layered vs. Cubic Li_xCoO_2. *J Electrochem Soc* **1998**, *145* (7), 2424–2431. https://doi.org/10.1149/1.1838653.

(17) Van der Ven, A.; Ceder, G. Electrochemical Properties of Spinel Li_xCoO_2 : A First-Principles Investigation. *Phys Rev B* **1999**, *59* (2), 742–749. https://doi.org/10.1103/PhysRevB.59.742.

(18) Kim, S.; I. Hegde, V.; Yao, Z.; Lu, Z.; Amsler, M.; He, J.; Hao, S.; R. Croy, J.; Lee, E.; M. Thackeray, M.; Wolverton, C. First-Principles Study of Lithium Cobalt Spinel Oxides: Correlating Structure and Electrochemistry. *ACS Applied Mater Interfaces* **2018**, *10* (16), 13479–13490. https://doi.org/10.1021/acsami.8b00394.

(19) Bai, J.; Sun, W.; Zhao, J.; Wang, D.; Xiao, P.; Young Peter Ko, J.; Huq, A.; Ceder, G.; Wang, F. Kinetic Pathways Templated by Low-Temperature Intermediates during Solid-State Synthesis of Layered Oxides. *Chem Mater* **2020**, *32* (23), 9906–9913. https://doi.org/10.1021/acs.chemmater.0c02568.

(20) Momma, K.; Izumi, F. *VESTA3* for Three-Dimensional Visualization of Crystal, Volumetric and Morphology Data. *J Appl Cryst* **2011**, *44* (6), 1272–1276. https://doi.org/10.1107/S0021889811038970.

(21) Amatucci, G. G.; Tarascon, J. M.; Larcher, D.; Klein, L. C. Synthesis of Electrochemically Active $LiCoO_2$ and $LiNiO_2$ at 100 °C. *Solid State Ion* **1996**, *84* (3–4), 169–180. https://doi.org/10.1016/0167-2738(96)00031-8.

(22) Okubo, M.; Hosono, E.; Kim, J.; Enomoto, M.; Kojima, N.; Kudo, T.; Zhou, H.; Honma, I. Nanosize Effect on High-Rate Li-Ion Intercalation in $LiCoO_2$ Electrode. *J Am Chem Soc* **2007**, *129* (23), 7444–7452. https://doi.org/10.1021/ja0681927.

(23) Larcher, D.; Palacín, M. R.; Amatucci, G. G.; Tarascon, J. -M. Electrochemically Active $LiCoO_2$ and $LiNiO_2$ Made by Cationic Exchange under Hydrothermal Conditions. *J Electrochem Soc* **1997**, *144* (2), 408. https://doi.org/10.1149/1.1837424.

(24) Tabuchi, M.; Ado, K.; Kobayashi, H.; Sakaebe, H.; Kageyama, H.; Masquelier, C.; Yonemura, M.; Hirano, A.; Kanno, R. Preparation of $LiCoO_2$ and $LiCo_{1-x}Fe_xO_2$ Using Hydrothermal Reactions. *J Mater Chem* **1999**, *9* (1), 199–204. https://doi.org/10.1039/A805311A.

(25) Song, S. W.; Han, K. S.; Sasagawa, I.; Watanabe, T.; Yoshimura, M. Effect of LiOH Concentration Change on Simultaneous Preparation of $LiCoO_2$ Film and Powder by Hydrothermal Method. *Solid State Ion* **2000**, *135* (1–4), 277–281. https://doi.org/10.1016/S0167-2738(00)00446-X.

(26) Adschirib, T.; Hakuta, Y.; Kanamura, K.; Arai, K. Continuous Production of $LiCoO_2$ Fine Crystals for Lithium Batteries by Hydrothermal Synthesis under Supercritical Condition. *High Press Res* **2001**, *20* (1–6), 373–384. https://doi.org/10.1080/08957950108206185.

(27) Burukhin, A.; Brylev, O.; Hany, P.; Churagulov, B. R. Hydrothermal Synthesis of $LiCoO_2$ for Lithium Rechargeable Batteries. *Solid State Ion* **2002**, *151* (1–4), 259–263. https://doi.org/10.1016/S0167-2738(02)00721-X.

(28) Teshima, K.; Lee, S.; Mizuno, Y.; Inagaki, H.; Hozumi, M.; Kohama, K.; Yubuta, K.; Shishido, T.; Oishi, S. Environmentally Friendly Growth of Well-Developed $LiCoO_2$ Crystals for Lithium-Ion Rechargeable Batteries Using a NaCl Flux. *Cryst Growth Des* **2010**, *10* (10), 4471–4475. https://doi.org/10.1021/cg100705d.

(29) Mizuno, Y.; Zettsu, N.; Yubuta, K.; Sakaguchi, T.; Saito, T.; Wagata, H.; Oishi, S.; Teshima, K. Fabrication of $LiCoO_2$ Crystal Layers Using a Flux Method and Their for Additive-Free Lithium-Ion Rechargeable Battery Cathodes. *Cryst Growth Des* **2014**, *14* (4), 1882–1887. https://doi.org/10.1021/cg5000217.

(30) Yoda, T.; Zettsu, N.; Onodera, H.; Mizuno, Y.; Kondo, H.; Teshima, K. Flux Growth of Patterned $LiCoO_2$ Crystal Arrays Directly on a Pt in Molten $LiNO_3$. *RSC Adv* **2015**, *5* (116), 96002–96007. https://doi.org/10.1039/c5ra17459g.

(31) Zettsu, N.; Nishikawa, K.; Yubuta, K.; Sakurai, K.; Yamamoto, Y.; Mizuno, Y.; Oishi, S.; Teshime, K. Flux Growth of Hexagonal Cylindrical $LiCoO_2$ Crystals Surrounded By-Ion Conducting Preferential Facets and Their Electrochemical Studied by Single-Particle Measurements. *J Mater Chem A Mater* **2015**, *3* (33), 17016–17021. https://doi.org/10.1039/c5ta02414e.

(32) Nishikawa, K.; Zettsu, N.; Teshima, K.; Kanamura, K. Intrinsic Electrochemical Characteristics in the Individual Needle-like $LiCoO_2$ Crystals Synthesized by Flux Growth. *Electrochemistry* **2017**, *85* (2), 72–76. https://doi.org/10.5796/electrochemistry.85.72.

(33) Izumi, F.; Momma, K. Three-Dimensional Visualization in Powder Diffraction. In *APPLIED CRYSTALLOGRAPHY XX*; Solid State Phenomena; Trans Tech Publications Ltd, 2007; Vol. 130, pp 15–20. https://doi.org/10.4028/www.scientific.net/SSP.130.15.

(34) Bale, C. W.; Pelton, A. D. Coupled Phase Diagram and Thermodynamic Analysis of the 18 Binary Systems Formed among Li_2CO_3, K_2CO_3, Na_2CO_3, LiOH, KOH, NaOH, Li_2SO_4, K_2SO_4 and Na_2SO_4. *Calphad* **1982**, *6* (4), 255–278. https://doi.org/10.1016/0364-5916(82)90020-7.

(35) Bale, C. W.; Bélisle, E.; Chartrand, P.; Decterov, S. A.; Eriksson, G.; Gheribi, A. E.; Hack, K.; Jung, I. H.; Kang, Y. B.; Melançon, J.; Pelton, A. D.; Petersen, S.; Robelin, C.; Sangster, J.; Spencer, P.; Van Ende, M. A. Reprint of: FactSage Thermochemical Software and Databases, 2010–2016. *Calphad* **2016**, *54*, 35–53. https://doi.org/10.1016/J.CALPHAD.2016.05.002.

(36) Lei, Y.; Li, X.; Liu, L.; Ceder, G. Synthesis and Stoichiometry of Different Layered Sodium Cobalt Oxides. *Chemistry of Materials* **2014**, *26* (18), 5288–5296. https://doi.org/10.1021/cm5021788.

(37) Matsui, M.; Mizukoshi, F.; Hasegawa, H.; Imanishi, N. Ca-Substituted P3-Type $Na_xNi_{1/3}Mn_{1/3}Co_{1/3}O_2$ as a Potential High Voltage Cathode Active Material for Sodium-Ion Batteries. *J Power Sources* **2021**, *485*, 229346. https://doi.org/10.1016/J.JPOWSOUR.2020.229346.

(38) Tournadre, F.; Croguennec, L.; Saadoune, I.; Carlier, D.; Shao-Horn, Y.; Willmann, P.; Delmas, C. On the Mechanism of the P2–$Na_{0.70}CoO_2$→O_2–$LiCoO_2$ Exchange Reaction—Part I: Proposition of a Model to Describe the P2–O2 Transition. *J Solid State Chem* **2004**, *177* (8), 2790–2802. https://doi.org/10.1016/J.JSSC.2004.04.027.

(39) Inaba, M.; Iriyama, Y.; Ogumi, Z.; Todzuka, Y.; Tasaka, A. Raman Study of Layered Rock-Salt $LiCoO_2$ and Its Electrochemical Lithium Deintercalation. *Journal of Raman Spectroscopy* **1997**, *28* (8), 613–617. https://doi.org/https://doi.org/10.1002/(SICI)1097-4555(199708)28:8<613::AID-JRS138>3.0.CO;2-T.

(40) V G Hadjiev; M N Iliev; I V Vergilov. The Raman Spectra of Co_3O_4. *Journal of Physics C: Solid State Physics* **1988**, *21* (7), L199. https://doi.org/10.1088/0022-3719/21/7/007.

(41) Akimoto, J.; Gotoh, Y.; Oosawa, Y. Synthesis and Structure Refinement of $LiCoO_2$ Single Crystals. *J Solid State Chem* **1998**, *141* (1), 298–302. https://doi.org/https://doi.org/10.1006/jssc.1998.7966.

Table of Contents

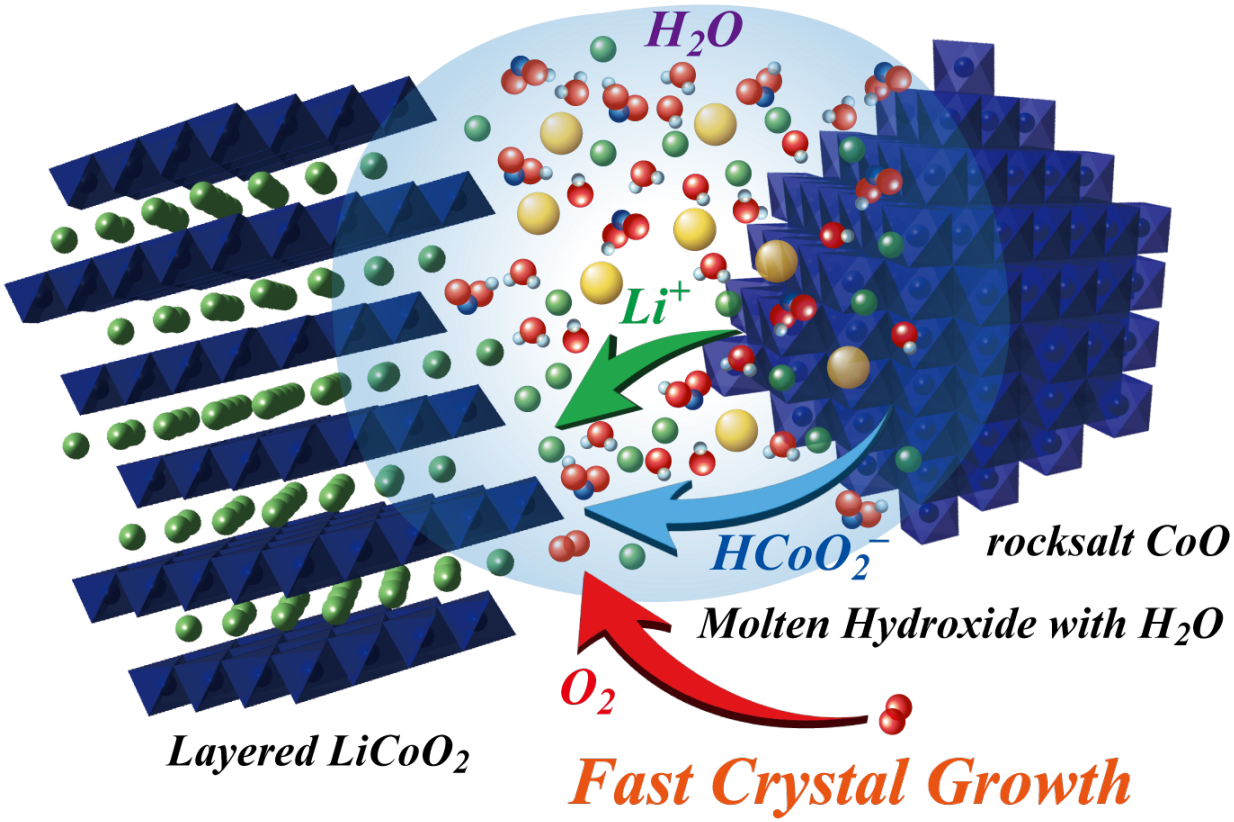

The reaction pathway to form the highly crystalline layered $LiCoO_2$. The rocksalt CoO is easily dissolved as $HCoO_2^-$ in a mixed molten alkaline hydroxide with excess water molecules. The dissolved $HCoO_2^-$ significantly accelerates the crystal growth of $LiCoO_2$ even at 300 °C.